

# Large-Eddy Simulation of Vortex Breakdown in Compressible Swirling Jet Flow

S. B. Müller<sup>†,\*</sup>, L. Kleiser<sup>†</sup>

<sup>†</sup>Institute of Fluid Dynamics, ETH Zürich, 8092 Zurich, Switzerland \*Email: se@ifd.mavt.ethz.ch

## ABSTRACT

*Vortex breakdown in compressible swirling jet flow is investigated by Large-Eddy Simulation (LES) based on the approximate deconvolution model (ADM) [8]. LES results are presented for a strongly swirling  $Ma = 0.6$  jet. Conditions are chosen similar to recent theoretical and experimental investigations by Gallaire & Chomaz [2] and Liang & Maxworthy [4], respectively.*

## INTRODUCTION

Swirling flows, both reacting and non-reacting, occur in many engineering applications. Curvature effects from the azimuthal component of velocity impose a radial pressure gradient and influence the development of the jet shear layer. Typical features of swirling jets include the development of complex recirculation zones, vortex breakdown, two or more states occurring at the same values of control parameters (bistability), and jump transition between flow states. These effects are of both fundamental and practical interest and are observed e. g. in tornadoes, over delta wings of aircraft and in vortex devices. Surprisingly, there is still no consensus on the explanation of the underlying mechanisms.

Accurate prediction of such flows by LES is a challenging task requiring accurate numerics and appropriate subgrid-scale models. In many cases the specification of boundary conditions is complicated because the upstream flow field is highly sensitive to downstream conditions. This sensitivity can even extend to the region near the nozzle inflow plane, making it a challenge to define suitable inflow and outflow conditions.

## NUMERICAL METHOD AND BOUNDARY CONDITIONS

Our computational code is based on a conservative formulation of the compressible Navier-Stokes equations expressed in generalized coordinates [1]. For the LES the convective as well as the diffusive terms are discretized using sixth to tenth-order (at interior points) compact central schemes [3].

We employ a mapping from Cartesian to cylindrical coordinates to retain the conservative formulation. This eliminates problems related to the specific numerical treatment of additional force terms (centrifugal and Coriolis force) that arise in other (e.g. weakly conservative) formulations. The centerline singularity of the governing equations is treated by a method proposed in [5]. This approach uses a shifted grid in the radial direction and thus avoids placing a grid point at the polar axis ( $r = 0$ ). In the azimuthal direction a Fourier spectral method is employed. Near the polar axis the azimuthal grid spacing becomes excessively fine due to the nature of the cylindrical coordinate system. To avoid unnecessarily small time steps, the number of re-

tained Fourier modes is linearly reduced towards the pole. The grid can be stretched in the radial and axial directions in order to adequately resolve regions with steep gradients. Time integration is done by a low-storage explicit third-order Runge-Kutta method. As a subgrid-scale model we use the approximate deconvolution model for compressible flows [8].

Special care is taken to define boundary conditions at the inflow plane that are suitable for swirling jet flow simulations. Disturbances are specified by amplified eigenmodes predicted by linear stability theory, for which a spatial, viscous linear stability tool has been developed [6,7]. At the lateral and outflow boundaries non-reflecting conditions (accounting for the curvilinear radial boundary) are employed and supplemented by sponge layers. The sponge layers at the inflow and outflow plane incorporate all five conservative variables. The mass flow rate at the outflow plane is specified and thus controls entrainment.

The governing equations are nondimensionalized using the jet radius  $r_0 = D_j/2$ , the jet exit velocity  $W_j$ , the ambient density  $\rho_\infty$ , the dynamic viscosity  $\mu_\infty$  and the ambient temperature  $T_\infty$ . The Reynolds number is given by  $Re = \rho_j W_j r_0 / \mu_j$ .

## RESULTS

In the following we report results for strongly swirling jets with and without forcing. Simulations were performed at Reynolds number  $Re = 5000$  and Mach number  $Ma = W_j/a_j = 0.6$ . The resolution was  $N_r \times N_\theta \times N_z = 181 \times 36 \times 145$  points spanning an integration domain of  $L_r/r_0 = 20$  and  $L_z/r_0 = 15$ . Analytical base flow profiles at the inflow for the mean axial and azimuthal velocity are specified as

$$w_B(r) = 1 / \left( 1 + \left( \exp \left( r^2 \log 2 \right) - 1 \right)^5 \right)$$

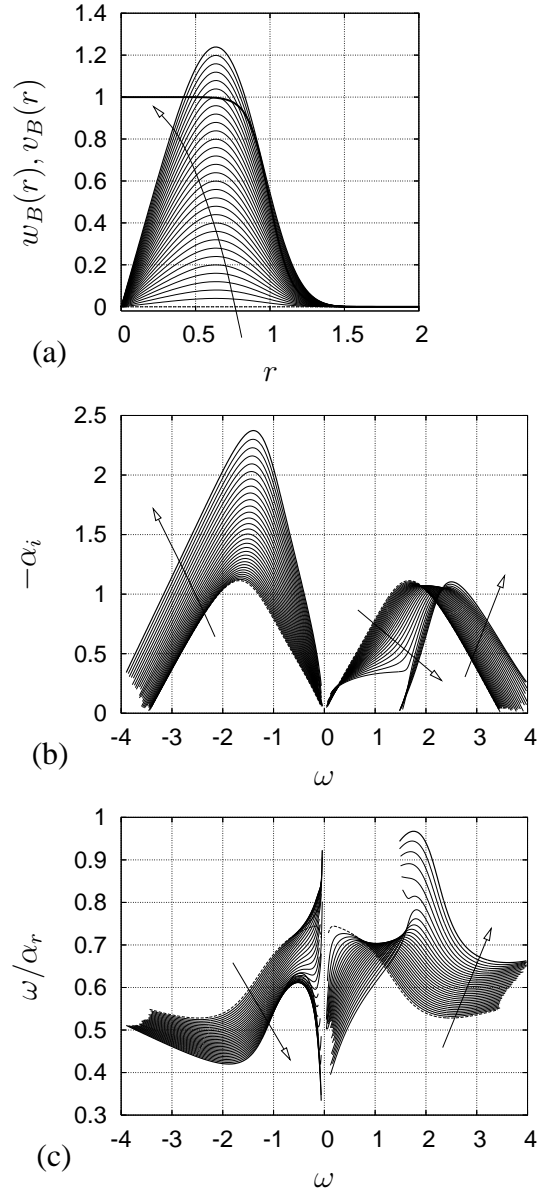


Fig. 1. Instability characteristics: (a) Axial and azimuthal base flow velocity profiles  $w_B(r)$  and  $v_B(r)$ , (b) spatial growth rates  $-\alpha_i$  for azimuthal wavenumber  $n = 1$  and (c) phase speeds  $\omega/\alpha_r$ . The arrows indicate the direction from zero ( ..... ) to maximum ( — ) swirl intensity  $s$ ,  $0 \leq s \leq 1$ .

and

$$v_B(r) = s \frac{5}{2} r \exp \left( - (r/r_v)^4 \right)$$

with  $r_v = 0.9$ . Assuming a uniform temperature  $T_B(r) = 1$  allows to compute the pressure distribution  $p_B(r)$  numerically using the momen-

tum equation in the radial direction

$$p_B(r) = p_B|_{r=0} \cdot \exp\left(\int_{\eta=0}^r \frac{\gamma Ma^2 v_B^2(\eta)}{\eta T_B(\eta)} d\eta\right).$$

Viscous spatial stability analysis for these inflow profiles was performed assuming traveling wave disturbances

$$\text{Re}\{\hat{q}(r) \exp(i(\alpha z + n\theta - \omega t))\}.$$

Further details of the linear stability solver may be found in [7]. By varying the strength of the swirl intensity  $s = i/31$ ,  $i = 0, \dots, 31$  we obtain stability characteristics for an azimuthal wavenumber  $n = 1$  as shown in figure 1. We performed two LES. The first one imposes a purely laminar base flow profile at the inflow plane using  $s = 1$  (unforced, self-excited jet) while the other incorporates an additional (4% amplitude) forcing consisting of the most dangerous helical  $n = 1$  instability (for  $s = 1$ ) in the positive frequency range (i. e. co-rotating instability at  $\omega_{\text{crit.}} \approx 2.5$ , which agrees almost exactly with the frequency of the solid body rotation part of the azimuthal velocity component). In both cases, the flow field was initially disturbed with small random fluctuations.

In the simulations, we observe a rapid deceleration of the axial velocity component within one jet diameter downstream of the inflow plane. A conical vortex breakdown develops with an initially laminar conical high-speed fluid sheet which first narrows with downstream distance from the inflow plane, see figure 2. Instabilities distort the sheet which finally breaks up into small-scale turbulence. The motion within the cone consists of recirculating currents that are weak compared to the motion within the sheet. Streamlines of velocity fields averaged in time (over a time interval of 60 dimensionless time units) as well as azimuthal direction are visualized in figure 3. Averaged velocity profiles for all three components as well as RMS fluctua-

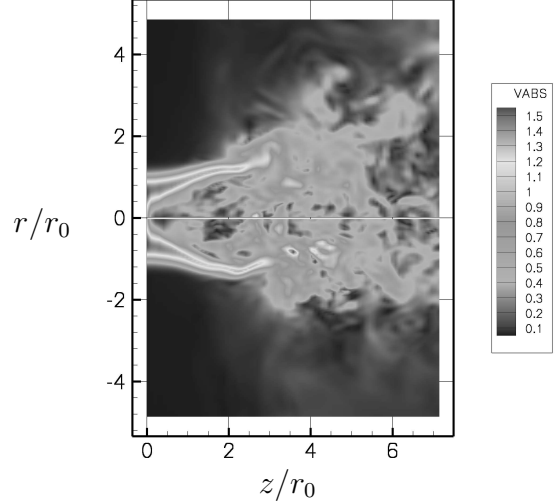


Fig. 2. Vortex breakdown in compressible swirling jet flow: contour plot of instantaneous velocity magnitude in the  $r$ - $z$ -plane at  $\theta = 0$ , self-excited jet.

tions are shown in figure 4. Compared to the flow features found in experiments by Liang & Maxworthy [4] for water flow at a Reynolds number of 500, the compressible breakdown exhibits a significantly faster deceleration of the centerline axial velocity. The deceleration is followed by a quite strong reverse flow in the axial direction downstream of the stagnation point. This phenomenon can be understood by considering the fact that according to the  $p_B(r)$  dependence derived above compressibility results in a larger ambient-to-jet pressure ratio compared to the incompressible limit. The RMS fluctuations in our case are much higher than in the experiments, especially near the centerline. This is attributed to the higher Reynolds number present in our simulations. The peaks of mean-velocity components as well as those of the RMS fluctuations are slightly shifted outwards by the forcing and accordingly, the cone angle is slightly increased by the forcing. However, the qualitative picture remains essentially unaltered by the forcing.

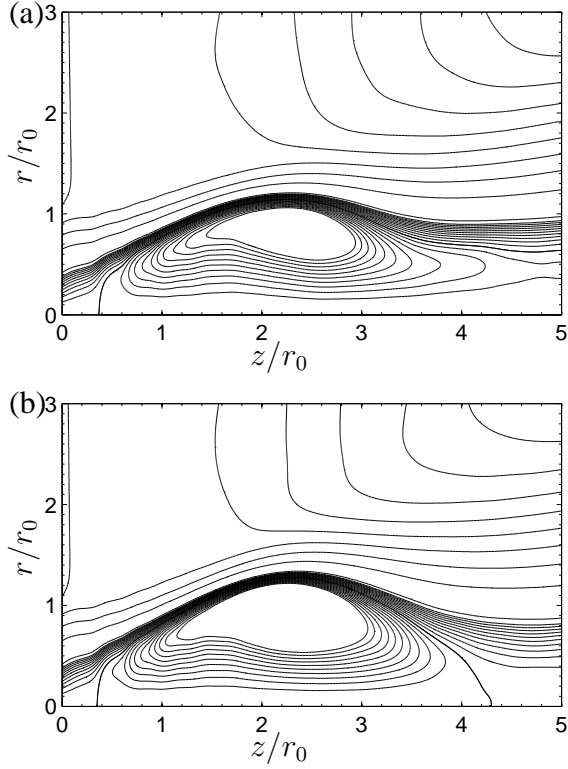


Fig. 3. Visualization of streamlines of averaged velocity: (a) self-excited jet, (b) forced jet.

The axial velocity component of instantaneous flow fields was Fourier transformed in the azimuthal direction and associated amplitudes for different wavenumbers  $n$  versus downstream coordinate are plotted in figure 5. The  $n = 1$  mode is initially dominant, closely followed by the  $n = 2$  mode. The higher modes ( $n > 7$ ) decrease monotonically with  $n$  as expected. The corresponding maximum locations of the  $n = 1$  mode within the  $r$ - $z$ -plane are plotted in figure 6. In the region near the inflow plane, the forced jet flow shows a growth of the  $n = 1$  mode that is consistent with linear theory. It exhibits a clearly visible helical instability co-rotating in time with the jet and with orientation of its inclination opposite to the mean swirl. In case of the self-excited jet, this instability structure is probably suppressed by the perfectly axisymmetric and laminar inflow profile. Nevertheless, the highest amount of turbulent energy of all helical waves is contained in the  $n = 1$  mode.

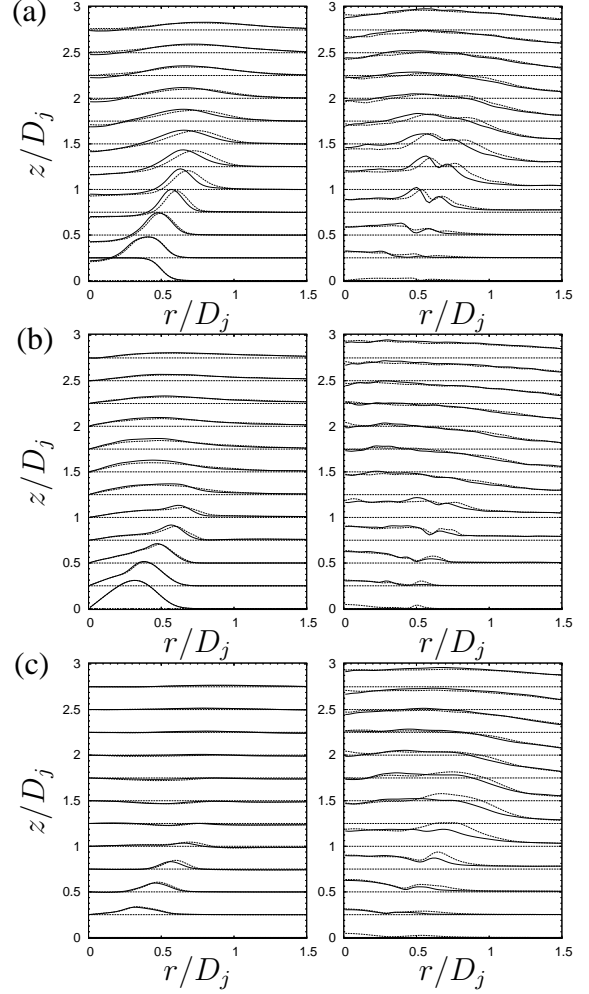


Fig. 4. Averaged flow statistics versus  $r/D_j$  at subsequent axial positions  $z/D_j$ . Left column: Favre-averaged mean velocity ( $\times 0.25$ ), right column: associated RMS fluctuations. (a) Axial velocity, (b) azimuthal velocity, (c) radial velocity. Self-excited jet (—) and forced jet (-----).

## CONCLUSIONS

The capability of the approximate deconvolution model to predict vortex breakdown of compressible swirling jet flow with massive swirl has been tested. The flow features include the formation of a cone and a recirculation zone. The simulations show good qualitative agreement with recent experimental results [4]. Spectral decompositions in space and time indicate that strong helical waves with low azimuthal

wavenumber support the destabilization and breakup of the cone sheet.

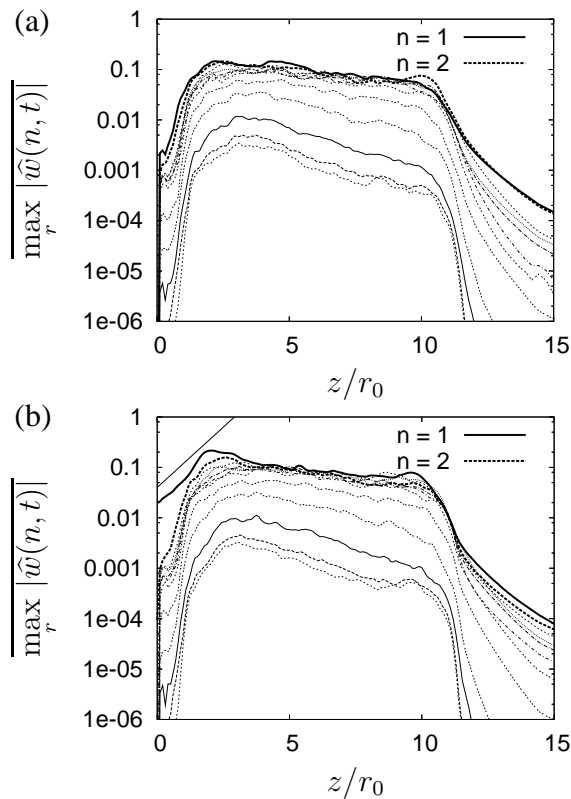


Fig. 5. Azimuthal Fourier amplitudes  $\max_r |\widehat{w}(n, t)|$  versus downstream coordinate  $z$ . (a) Self-excited jet, (b) forced jet. The solid line in (b) shows the growth rate of the forced  $n = 1$  mode predicted by linear stability theory.

## BIBLIOGRAPHY

- [1] N. A. Adams. Direct simulation of the turbulent boundary layer along a compression ramp at  $M = 3$  and  $Re_\theta = 1685$ . *J. Fluid Mech.*, 420:47–83, 2000.
- [2] F. Gallaire and J. M. Chomaz. Mode selection in swirling jet experiments: a linear stability analysis. *J. Fluid Mech.*, 494:223–253, 2003.
- [3] S. K. Lele. Compact finite difference schemes with spectral-like resolution. *J. Comput. Phys.*, 103:16–42, 1992.

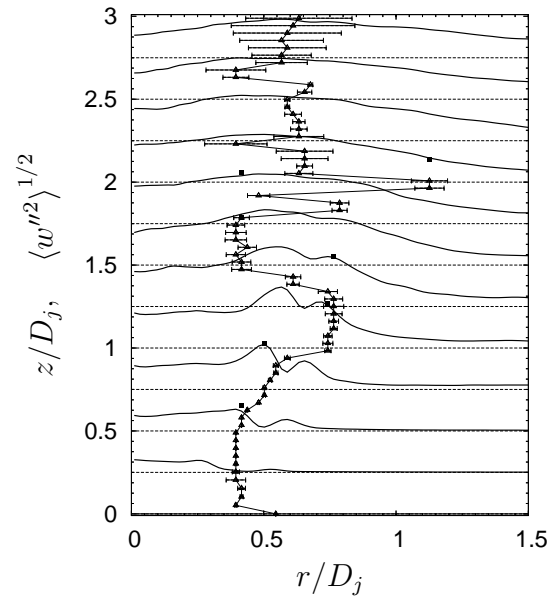


Fig. 6. Self-excited jet: RMS fluctuations of axial velocity and temporal average of radial location of  $n = 1$  peaks versus  $r/D_j$  at subsequent axial positions. The errorbar indicates temporal band of peak locations.

- [4] H. Liang and T. Maxworthy. An experimental investigation of swirling jets. *J. Fluid Mech.*, 525:115–159, 2005.
- [5] K. Mohseni and T. Colonius. Numerical treatment of polar coordinate singularities. *J. Comput. Phys.*, 157:787–795, 2000.
- [6] S. B. Müller, F. Keiderling, and L. Kleiser. Viscous compressible stability investigations in cylindrical coordinates. In *Proc. Appl. Math. Mech.*, pages 466–467, 2004. DOI: 10.1002/pamm.200410215.
- [7] S. B. Müller and L. Kleiser. Spatial linear stability analysis of compressible swirling jet flow. 2005. To be submitted.
- [8] S. Stolz, N. A. Adams, and L. Kleiser. The approximate deconvolution model for LES of compressible flows and its application to shock-turbulent-boundary-layer interaction. *Phys. Fluids*, 13(6):2985–3001, 2001.